CENTRE FOR **STOCHASTIC GEOMETRY**
AND ADVANCED **BIOIMAGING**

Ali Hoseinpoor Rafati, Johanna F. Ziegel, Jens R. Nyengaard
and Eva B. Vedel Jensen

Stereological Estimation of Particle Shape and Orientation From Volume Tensors

No. 12, September 2015

source: https://doi.org/10.7892/boris.76071 | downloaded: 12.10.2024

Stereological Estimation of Particle Shape and Orientation From Volume Tensors

Ali Hoseinpoor Rafati[1], Johanna F. Ziegel[2], Jens R. Nyengaard[1] and Eva B. Vedel Jensen[3]

[1]Stereological Research Laboratory, Aarhus University
[2]Department of Mathematics and Statistics, University of Bern
[3]Department of Mathematics, Aarhus University

Summary

In the present paper, we describe new robust methods of estimating cell shape and orientation in 3D from sections. The descriptors of 3D cell shape and orientation are based on volume tensors which are used to construct an ellipsoid, the Miles ellipsoid, approximating the average cell shape and orientation in 3D. The estimators of volume tensors are based on observations in several optical planes through sampled cells. This type of geometric sampling design is known as the optical rotator. The statistical behaviour of the estimator of the Miles ellipsoid is studied under a flexible model for 3D cell shape and orientation. In a simulation study, the lengths of the axes of the Miles ellipsoid can be estimated with CVs of about 2% if 100 cells are sampled. Finally, we illustrate the use of the developed methods in an example, involving neurons in the medial prefrontal cortex of rat.

1 Introduction

Robust methods for estimating cell shape and orientation are a prerequisite for the detailed analysis of the architecture of biological tissue. As shown recently in [12], volume tensors provide a concise set of descriptors of cell shape and orientation in 3D as well as cell size and position. These tensors can, in contrast to scalar shape measures, describe anisotropic structures, e.g. cells being elongated in a specific direction in 3D.

The volume tensor of rank 0 is simply the volume of the cell, while a normalized version of the volume tensor of rank 1 is the centre of gravity. By combining the volume tensors of rank 0, 1 and 2, an ellipsoidal approximation to the cell can be constructed that summarizes its shape and orientation in 3D, see [12].

When studying cell populations by microscopy, an extra challenge is that cells might not be observable directly, but only via sections. An important contribution in [12] is the development of estimators of volume tensors that combine observations in

several optical planes through sampled cells, but avoid observations in the peripheral parts of the cells. This type of geometric sampling design, called the optical rotator, was already introduced in [10] for estimation of cell volume and surface area. The estimators developed in [12] are local stereological estimators, since measurements on a sampled cell are relative to a reference point of the cell, typically the nucleus of the cell. See [1] for a general introduction to stereology and [6] for details on local stereology.

In the simpler situation where the spatial structure under study can be observed directly and not only via sections, volume tensors, or more generally Minkowski tensors, have already been used succesfully in material science as shape descriptors ([3], [4], [8], [9]) and also to some extent in the biosciences ([2]). In [11], shape and orientation of 2D sections of neurons are analyzed, without relating the results to the analogous quantities in 3D.

The principal purpose of this paper is to describe the robust estimation of volume tensors from optical microscopy images, making these methods available to scientists working in microscopy. For cell populations, the 3D shape and orientation of the typical cell will be described by the so-called Miles ellipsoid ([12]) which can be estimated from the volume tensors of a sample of cells. (The Miles ellipsoid is named after Roger Miles who was amongst the first to introduce geometric sampling theory in stereology.) If all cells have the same shape and orientation, then the Miles ellipsoid can be regarded as an ellipsoidal approximation to such a cell. In the more general situation where cells have varying shape and orientation, the Miles ellipsoid contains information about the average cell shape and orientation.

As a new contribution in the present paper, we study the statistical behaviour of the estimator of the Miles ellipsoid under a flexible model for 3D cell shape and orientation. The simulation study shows that the estimator is well-behaved. In particular, the lengths of the axes of the Miles ellipsoid can be estimated with CVs of about 2% if 100 cells are sampled. Finally, we illustrate the use of the developed methods in an example, involving neurons in the medial prefrontal cortex of rat.

In the remaining part of the paper, we will refer to 'particles' instead of 'cells', to emphasize that the methods are generally applicable. The paper is organized as follows. In Section 2, volume tensors are presented. Section 3 shows how the volume tensors can be estimated, using the optical rotator design. In Section 4, inference for particle populations is discussed, using a design-based or a model-based approach, and the example is presented in Section 5. Perspectives are discussed in Section 6, while some derivations are deferred to an Appendix.

2 Volume tensors

Let K be a particle (compact subset of $\mathbb{R}^3$). We can associate to K a collection of volume tensors. We will focus on the volume tensors of rank 0, 1 and 2.

The volume tensor $T_0(K)$ of rank 0 is simply the volume $v(K)$ of K while a normalized version of the volume tensor $T_1(K)$ of rank 1 is the centre of gravity

of K. More specifically, the volume tensor of rank 1 is the point in $\mathbb{R}^3$ defined by

$$T_1(K) = \int_K x \, \mathrm{d}x.$$

Here, $x = (x_1, x_2, x_3)$ and the integration is to be understood coordinate-wise. The ith coordinate of $T_1(K)$ is thus

$$T_1(K)_i = \int_K x_i \, \mathrm{d}x_1 \, \mathrm{d}x_2 \, \mathrm{d}x_3,$$

$i = 1, 2, 3$. The centre of gravity of K is $c(K) = T_1(K)/T_0(K)$.

Information about the shape and orientation of K can be obtained by combining $T_0(K)$ and $T_1(K)$ with the volume tensor $T_2(K)$ of rank 2 which is the following 3×3 matrix

$$T_2(K) = \frac{1}{2} \int_K x^2 \, \mathrm{d}x.$$

Here, x^2 is the symmetric tensor of rank 2 induced by x, i.e. the 3×3 matrix with entries $(x^2)_{i,j} = x_i x_j$, $i, j = 1, 2, 3$. Again, the integration is to be understood coordinate-wise such that the (i, j)th entry of $T_2(K)$ is

$$T_2(K)_{i,j} = \frac{1}{2} \int_K x_i x_j \, \mathrm{d}x_1 \, \mathrm{d}x_2 \, \mathrm{d}x_3,$$

$i, j = 1, 2, 3$.

The volume tensors $T_0(K)$, $T_1(K)$ and $T_2(K)$ can be used to construct an ellipsoidal approximation to K of the form $c(K)+e(K)$, where $e(K)$ is a centred ellipsoid with the same volume as K, which captures shape and orientation properties of K, see Figure 1. If K is actually an ellipsoid, then $K = c(K) + e(K)$.

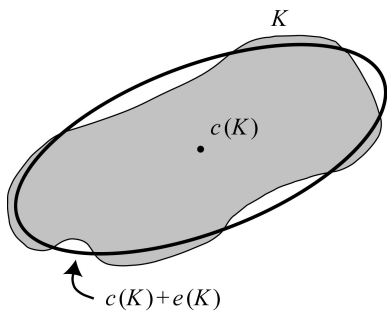

Figure 1: 2D illustration of the ellipsoidal approximation to a particle K. Here, $c(K)$ is the centre of gravity and $e(K)$ is a centred ellipsoid, approximating $K - c(K)$. If K is an ellipsoid, $K = c(K) + e(K)$.

The ellipsoid $e(K)$ depends on the volume of K and the volume tensor of rank 2 of $K - c(K)$

$$T_2(K - c(K)) = T_2(K) - \frac{T_1(K)^2}{2T_0(K)}.$$

Let

$$T_2(K - c(K)) = B \Lambda B^T$$

be the spectral decomposition of $T_2(K - c(K))$ where B is an orthogonal matrix and Λ is a diagonal matrix with diagonal elements λ_i, $i = 1, 2, 3$. (Since T_2 is positive semi-definite, $\lambda_i \geq 0$.) Then, the directions of the semi-axes of $e(K)$ are the columns of B and the lengths of the semi-axes of $e(K)$ are proportional to $\sqrt{\lambda_i}$, $i = 1, 2, 3$. The size of $e(K)$ is determined by the requirement that K and $e(K)$ have the same volume.

3 Estimation using the optical rotator

The volume tensors of K may be estimated unbiasedly using an optical rotator design, see [10, 12]. An optical rotator is an optical slice of thickness $2t$, say, centred at a reference point of the particle, taken here to be the origin O, see Figure 2. The slice is uniformly rotated around a fixed axis passing through the reference point O in the midplane. In the literature, see e.g. [10], the axis is called the vertical axis (VA), although the axis need not be vertical. Accordingly, the optical slice is called a vertical optical rotator. The slice is subsampled by a systematic set of optical planes parallel to the slice and the planar profiles are subsequently subsampled by line grids placed alternatingly parallel and perpendicular to VA, see Figure 2.

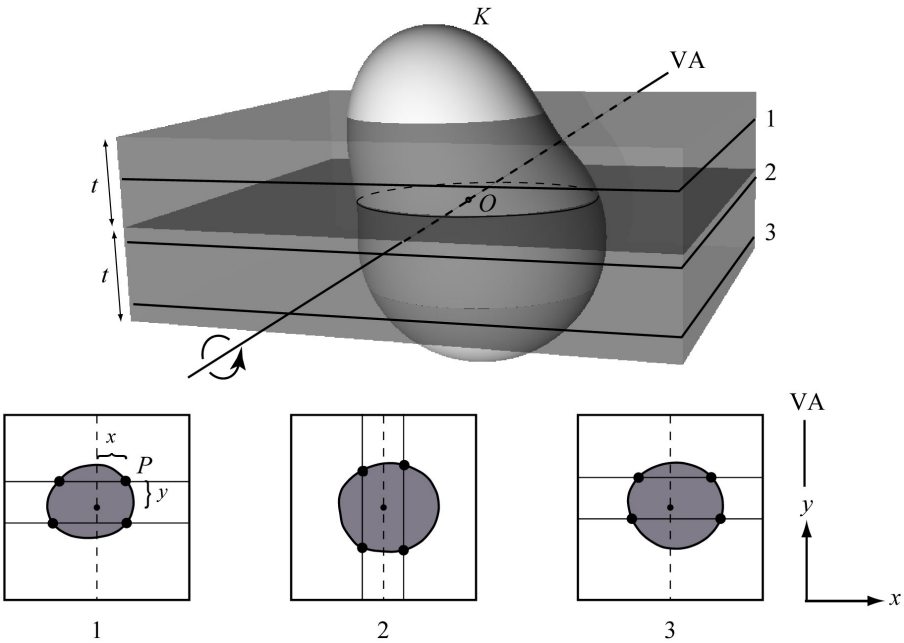

Figure 2: (Upper) The particle K is sectioned by an optical vertical random slice of thickness $2t$, obtained by a uniform rotation around the vertical axis VA passing through the reference point O in the midplane (dark plane). The slice is subsampled by a systematic set (1, 2, 3) of optical planes parallel to the slice. (Lower) In the planes with known distance z to O, the planar profiles are subsampled, using line grids placed alternatingly parallel and perpendicular to VA. The coordinates (x, y, z) of the intersection points P (indicated by $\bullet$) between the boundary of K and each line is recorded. In the illustration, the vertical axis (stippled) passing through the projection of O onto the planes is also shown.

Now, let P be the notation used for an intersection point between the boundary

of K and a line within a plane in the optical slice through K. Let the intersection between K and such a line consist of a collection of line segments $[P_{k-}, P_{k+}]$. Then, the volume tensors of rank 0, 1 and 2 can be estimated unbiasedly as

$$\widetilde{T}_0(K) = a \sum_k [g_0(P_{k+}) - g_0(P_{k-})], \tag{3.1}$$

$$\widetilde{T}_1(K) = a \sum_k [g_1(P_{k+}) - g_1(P_{k-})], \tag{3.2}$$

$$\widetilde{T}_2(K) = a \sum_k [g_2(P_{k+}) - g_2(P_{k-})], \tag{3.3}$$

see the Appendix and [12]. Here, a is the area associated with one line, i.e. the product of the distance between neighbour planes and the distance between neighbour lines within a plane. Below, we give the g-functions for a point P with coordinates (x, y, z) in the coordinate system where the y-axis is the 'vertical axis', the x-axis is parallel to the slice and the z-axis is perpendicular to the slice. More details are given in the Appendix.

Lines parallel to the vertical axis. The g-functions depend here on the function $F_{1,1}$ which is the distribution function of the beta-distribution with parameters $\alpha = \beta = 1/2$. More specifically,

$$F_{1,1}(u) = \begin{cases} 0 & \text{if } u < 0, \\ \frac{2}{\pi} \arcsin(\sqrt{u}) & \text{if } 0 \le u \le 1, \\ 1 & \text{if } u > 1. \end{cases}$$

We have

$$g_0(x, y, z) = F_{1,1}\left(\frac{t^2}{x^2 + z^2}\right)^{-1} y, \tag{3.4}$$

$$g_1(x, y, z) = F_{1,1}\left(\frac{t^2}{x^2 + z^2}\right)^{-1} (xy, \tfrac{1}{2}y^2, yz), \tag{3.5}$$

$$g_2(x, y, z) = \frac{1}{2} F_{1,1}\left(\frac{t^2}{x^2 + z^2}\right)^{-1} \begin{pmatrix} yx^2 & \frac{1}{2}y^2x & xyz \\ \frac{1}{2}y^2x & \frac{1}{3}y^3 & \frac{1}{2}y^2z \\ xyz & \frac{1}{2}y^2z & yz^2 \end{pmatrix}. \tag{3.6}$$

Lines perpendicular to the vertical axis. In this case, the g-functions depend on a function of two variables

$$f_s(x, z) = \int_0^x u^s F_{1,1}\left(\frac{t^2}{u^2 + z^2}\right)^{-1} \mathrm{d}u,$$

where the index s may take the values $s = 0, 1, 2$. This function cannot be integrated explicitly, but numerical integration can be used. We have

$$g_0(x, y, z) = f_0(x, z), \tag{3.7}$$

$$g_1(x, y, z) = (f_1(x, z), f_0(x, z)y, f_0(x, z)z), \tag{3.8}$$

$$g_2(x, y, z) = \frac{1}{2} \begin{pmatrix} f_2(x, z) & f_1(x, z)y & f_1(x, z)z \\ f_1(x, z)y & f_0(x, z)y^2 & f_0(x, z)yz \\ f_1(x, z)z & f_0(x, z)yz & f_0(x, z)z^2 \end{pmatrix}. \tag{3.9}$$

Note that the estimators of the volume obtained by using the g_0-functions already appeared in [10], but with a different notation. Thus, the formulae for the case of lines parallel to the vertical axis, appearing in [10, (4a), (4b)], are obtained by replacing y in (3.4) by d_1 and $x^2 + z^2$ by d_2^2, while the formulae for the case of lines perpendicular to the vertical axis, appearing in [10, (5a), (5b), (5c)], are obtained by replacing x in (3.7) by d_1.

4 Inference for particle populations

4.1 Design-based approach

4.1.1 The displacement vector $\bar{c}$ and the Miles ellipsoid $\bar{e}$

Let the particle population consist of N particles $K_1, \ldots, K_N$. We assume that we can associate a reference point $x(K) \in K$ to each particle K. The reference point $x(K)$ will be used as the origin of K. We let

$$\bar{T}_k = \frac{1}{N} \sum_{i=1}^{N} T_k(K_i - x(K_i)), \quad k = 0, 1, 2,$$

be the mean particle volume tensor of rank k, where each particle K_i enters with its own reference point $x(K_i)$ as origin. For $k = 0$, we get the mean particle volume $\bar{v} = \bar{T}_0$ while the vector $\bar{c} = \bar{T}_1/\bar{T}_0$, called the *displacement vector*, contains information about the difference between the centre of gravity and the reference point for a typical particle, see Figure 3.

Likewise, we can construct an approximating ellipsoid $\bar{c} + \bar{e}$ that contains information about particle shape and orientation of the typical particle. Here, $\bar{e}$ is a centred ellipsoid that can be constructed from $\bar{T}_0$, $\bar{T}_1$ and $\bar{T}_2$, using exactly the same procedure as the one used for constructing $e(K)$ from $T_0(K)$, $T_1(K)$ and $T_2(K)$. The ellipsoid $\bar{e}$ is called the *Miles ellipsoid*. If all particles K_i are translates of the same particle K_0, say, then $\bar{e} = e(K_0)$.

Interpretations of the Miles ellipsoid are also illustrated in Figure 3 where the four rows show different situations: particles with (A) identical position of the reference point relative to the centre of gravity, and identical shape and orientation, (B) displacement vector equal to the origin, and identical shape and orientation, (C) identical position of the reference point relative to the centre of gravity, identical shape, but varying orientation, and (D) identical position of the reference point relative to the centre of gravity, varying shape, but identical orientation.

4.1.2 Sampling of particles

In order to estimate the mean particle volume, the displacement vector and the Miles ellipsoid, we need to collect a uniform random sample of particles where each particle has the same probability of being sampled.

A well-established approach in microscopy is to cut the region of interest, containing the particles, into m blocks, say, and from each of these blocks select a

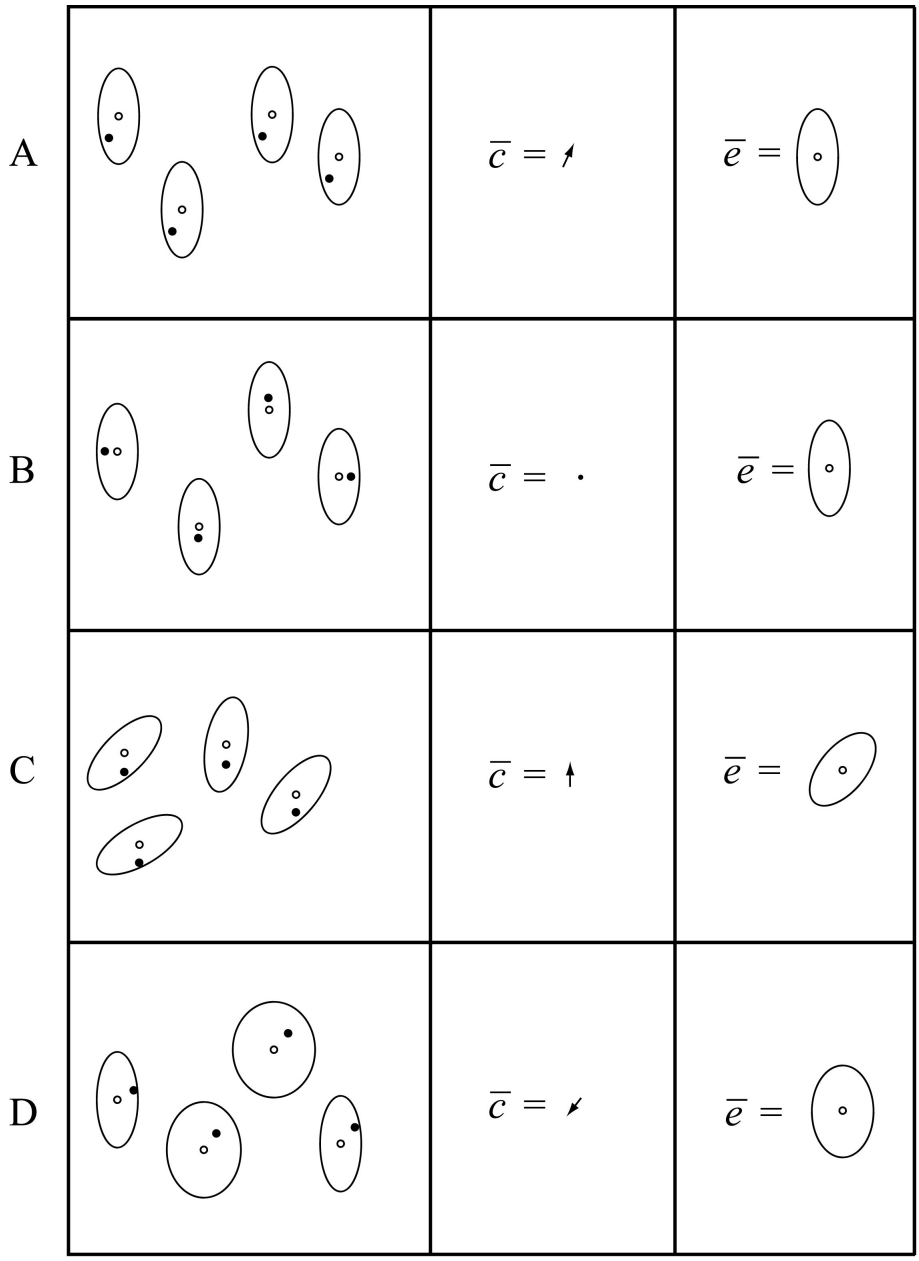

Figure 3: Interpretation of the displacement vector $\bar{c}$ and the Miles ellipsoid $\bar{e}$. The left column shows elliptic particles with their centre of gravity indicated by an open circle and their reference point by a closed circle. The middle column shows the displacement vector $\bar{c}$, i.e. the average vector pointing from the reference point to the centre of gravity. The right column shows the Miles ellipse $\bar{e}$, i.e. the average shape and orientation of the particles shown to the left.

systematic stack of parallel vertical uniform random thick sections. Systematic random sampling of particles is performed within each sampled thick section, using optical disectors, see e.g. [1, Chapter 10 and 12] and references therein. A particle is sampled if its reference point appears within the quadratic counting frame of the disector. Measurements on each sampled particle are performed, using an optical rotator, as described in Section 3.

Since the displacement vector and the Miles ellipsoid must be specified in a specific coordinate system, it is important to keep track of the sampling such that the local coordinate system centred at the reference point of a sampled particle can be translated into the same coordinate system for all sampled particles. This requirement may be relaxed if the particles can be modelled by a random particle process obeying certain invariance properties, see Section 4.2 below on the model-based approach. A procedure for keeping track of local coordinate systems is sketched in Figure 4.

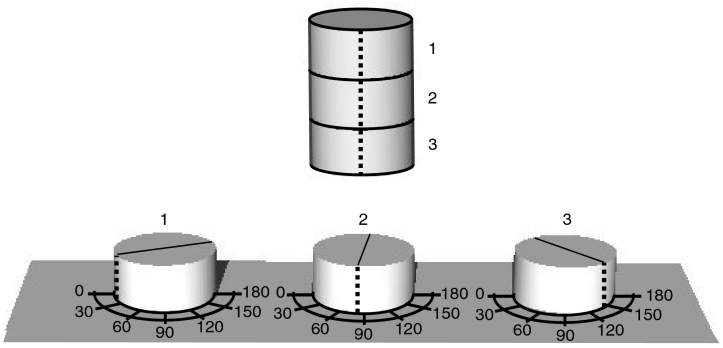

Figure 4: (Upper) The cylinder containing the particles are cut into three blocks (1, 2, 3). Their relative position is indicated by the stippled vertical line. (Lower) A systematic stack of parallel vertical uniform random thick sections is cut within each block. The sections are all parallel to a vertical plane rotated an angle θ where $\theta = 20^o$, 80°, 140° for blocks 1, 2, 3, respectively. The first angle has been chosen uniform randomly in the interval $[0^o, 60^o)$ and the subsequent angles are then chosen systematically.

4.1.3 Estimation of $\bar{v}$, $\bar{c}$ and $\bar{e}$

Let $S \subset \{1, \ldots, N\}$ be the random sample of particles of size n, say. Then,

$$\widehat{T}_k = \frac{1}{n} \sum_{i \in S} \widetilde{T}_k(K_i - x(K_i))$$

is a ratio-unbiased estimator of the mean particle volume tensor of rank k, $\bar{T}_k$. The mean particle volume can then be estimated by $\widehat{v} = \widehat{T}_0$ and the displacement vector by $\widehat{c} = \widehat{T}_1/\widehat{T}_0$. Finally, an estimator $\widehat{e}$ of the Miles ellipsoid can be constructed from $\widehat{T}_0$, $\widehat{T}_1$ and $\widehat{T}_2$, using exactly the same procedure as the one used in Section 2 for constructing $e(K)$ from $T_0(K)$, $T_1(K)$ and $T_2(K)$.

When applying these estimators in a concrete situation, an important question is how many particles need to be sampled in order to obtain a given precision of the

estimators. The answer to this question depends of course on the distribution of the particles in the containing space.

In order to get some insight into this problem, a simulation study was conducted where all particles were translates of the same particle K_0 which was an ellipsoid with axes parallel to the coordinate axes and lengths of semi-axes equal to $a = 8$, $b = 4$, $c = 3$. The coordinates of the displacement vector were $(-1.7, 1.7, 1.0)$. The optical rotator was designed so that the distance between planes and lines, respectively, imitated the ones used in the example discussed in Section 5.

Table 1 shows the mean and CV of the estimated semi-axes lengths of the Miles ellipsoid, based on measurements in optical rotators through $n = 5, 10, 20, 50$ sampled particles. A total of 100000 independent optical rotators were simulated so the number of simulations of measurements from n particles was $100000/n$. Already for $n = 10$ particles, the biases are negligable. The CVs are less than 10% if at least 20 particles are sampled.

n	5	10	20	50
a	7.815 (0.181)	7.903 (0.125)	7.951 (0.087)	7.981 (0.054)
b	4.074 (0.057)	4.034 (0.042)	4.016 (0.031)	4.006 (0.020)
c	2.985 (0.055)	2.994 (0.036)	2.997 (0.025)	2.998 (0.015)

Table 1: Mean (and CV) of the estimated semi-axes lengths of the Miles ellipsoid, based on measurements in optical rotators through n sampled particles. The true Miles ellipsoid is parallel to the coordinate axes and has $a = 8$, $b = 4$, $c = 3$. The vertical axis was in this coordinate system spanned by $u = (0.224, 0.919, 0.324)$. The thickness of the slice used in the optical rotators was $2t$ with $t = 2.5$, the slice was subsampled by three planes and the distance between neighbour lines within a plane was 4.

These results should be handled with care. The particle population consists of particles that all are translates of the same ellipsoid K_0. Therefore, parallel optical rotators through sampled particles contain the same information. Usually, in optical microscopy, all optical rotators within a block are parallel. Accordingly, the number of independent optical rotators is equal to the number of blocks. In such a sampling situation, the results in Table 1 should refer to n blocks rather than n particles, as confirmed by simulation (not shown here).

The simulation results may also be used to emphasize that the estimators (3.1)–(3.3) of volume tensors for a single particle K are unbiased, but may have large variances in real practical sampling designs. As a consequence, the resulting estimators of the centre of gravity $c(K)$ and the approximating ellipsoid $e(K)$ for a single particle K may have a non-negligible bias since the operations needed for calculating these quantities from the volume tensors are non-linear.

This is indeed the case as confirmed by the simulation study. For each of the 100000 simulated optical rotators, estimates of the lengths of the semi-axes were calculated from $\widetilde{T}_0$, $\widetilde{T}_1$ and $\widetilde{T}_2$ given at (3.1)-(3.3). They had mean and CV as

follows

$$\bar{a} = 8.592, \qquad CV = 0.43,$$
$$\bar{b} = 4.841, \qquad CV = 0.20,$$
$$\bar{c} = 3.129, \qquad CV = 0.18.$$

In Figure 5, histograms of the estimates of a, b and c are shown.

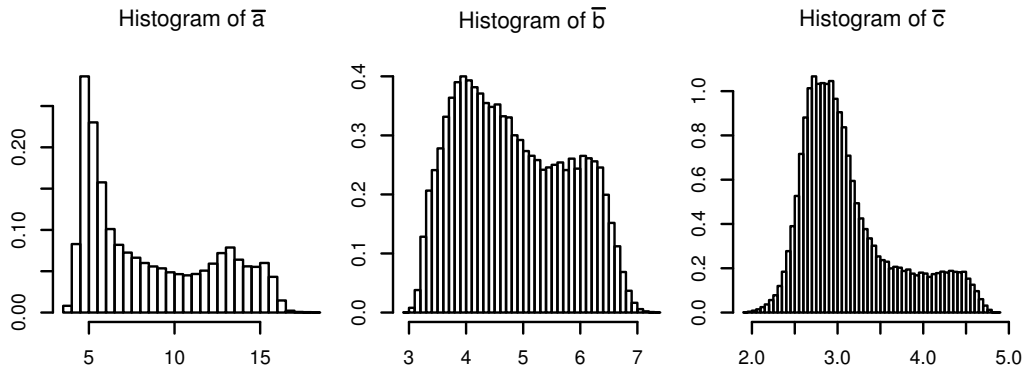

Figure 5: Histograms of estimates of a, b and c based on observations from 100000 vertical optical rotators. The true values are $a = 8$, $b = 4$ and $c = 3$. For more details, see text.

The estimators of the semi-axis lengths are biased by 7%, 21% and 4%, respectively. This bias can be reduced by increasing the slice thickness t of the optical rotator, but this is typically not feasible in optical microscopy due to overprojection. As a consequence, the simulation study indicates that in real practical sampling designs it is not likely that we can get precise information about $c(K)$ and $e(K)$ for a single particle K. This phenomenon is well-known from local stereological estimation of particle volume. It is usually not possible to get a precise estimate of the volume $v(K)$ of a single particle K.

4.2 Model-based approach

In some applications, it is impossible to take a purely design-based approach because the involved random sampling is impracticable, e.g. because the observer looses track of the structure under the devised random sampling.

In such cases, the estimators developed above may still be used on a sample of particles in an arbitrary 3D sampling window if the particles can be regarded as part of a realization of a stationary particle process with a particle distribution, invariant under rotation around a fixed axis L_1. Then, it is not needed to uniformly rotate optical rotators around this axis. The Miles ellipsoid is under this restricted isotropy assumption an ellipsoid of revolution around L_1, called the vertical axis. For more details about the model-based approach, see [12, p. 824-827].

We have investigated by simulation the statistical properties of an estimator of the Miles ellipsoid for the case of restricted isotropy. Under this invariance assumption, it can be shown that

$$\bar{T}_2 - \frac{(\bar{T}_1)^2}{2\bar{T}_0}$$

has a spectral decomposition of the form $B\Lambda B^T$ where B is known and the diagonal elements λ_2 and λ_3 of Λ are equal, $\lambda_2 = \lambda_3 = \lambda_{23}$, say. The parameters λ_1 and λ_{23} can be estimated by minimizing the Frobenius norm

$$\left\| \widehat{T}_2 - \frac{(\widehat{T}_1)^2}{2\widehat{T}_0} - B \begin{pmatrix} \lambda_1 & 0 & 0 \\ 0 & \lambda_{23} & 0 \\ 0 & 0 & \lambda_{23} \end{pmatrix} B^T \right\|^2$$

with respect to λ_1 and λ_{23}. The estimated Miles ellipsoid is an ellipsoid of revolution around the vertical axis with volume $\widehat{T}_0$, semi-axis length along the vertical axis proportional to $\widehat{\lambda}_1^{1/2}$ and semi-axis lengths perpendicular to the vertical axis proportional to $\widehat{\lambda}_{23}^{1/2}$.

In the simulation study, we used the flexible stochastic particle model developed in [12, p. 824-826]. The particles are random deformations of a fixed particle K_0. They are star-shaped with respect to their reference points and have radial functions R relative to their reference points of the form

$$R(u) = M(u)\varepsilon(u), \quad u \in \mathbb{S}^2. \tag{4.1}$$

Here, $R(u)$ is the distance from the reference point to the boundary of the particle in direction u, represented as a point on the unit sphere $\mathbb{S}^2$. Furthermore, M is the radial function of the fixed star-shaped set K_0 and ε is a so-called Lévy-based isotropic random field on $\mathbb{S}^2$, see [12, p. 825]. The parameters of the random field ε are chosen such that the mean particle volume is equal to the volume of the fixed particle K_0.

Particles simulated from this model as deformations of a prolate ellipsoid K_0 are shown in Figure 6. The ellipsoid is shown to the left, followed by five random deformations. Since such a K_0 is invariant under rotation around its longest axis, the particle distribution is also invariant under rotation around this axis. It can be shown that the Miles ellipsoid is equal to K_0.

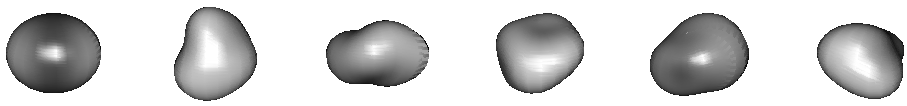

Figure 6: Particles simulated under the stochastic particle model (4.1) as random deformations of a prolate ellipsoid with longest axis in direction $(0.987, -0.162, 0)$ and semi-axis lengths 5.866 and 4.968, respectively. The displacement vector is $(-0.111, -0.224, 0.069)$. The ellipsoid is shown to the left, followed by five random deformations.

In Table 2, the mean and CV of the semi-axis lengths of the estimated Miles ellipsoid, determined from estimated mean volume tensors $\widehat{T}_0$, $\widehat{T}_1$ and $\widehat{T}_2$ based on $n = 10, 20, 50, 100$ particles in 5000 simulations, are shown. A CV of about 2% is obtained when 100 particles are sampled. Note that since the particle distribution is invariant under rotation around the vertical axis, the total number of sampled particles is the determining factor for the precision of the estimates. However, it is important to estimate the Miles ellipsoid under the restricted isotropy assumption. If it is attempted to estimate a general ellipsoid, using optical rotators with as few as 2 rotation angles, the resulting estimator is not well-behaved.

n	10	20	50	100
a	5.882 (0.083)	5.878 (0.060)	5.871 (0.039)	5.870 (0.028)
$b = c$	4.956 (0.066)	4.958 (0.048)	4.965 (0.031)	4.966 (0.022)

Table 2: Mean (and CV) of the semi-axis lengths of the estimated Miles ellipsoid, determined from estimated mean volume tensors $\widehat{T}_0$, $\widehat{T}_1$ and $\widehat{T}_2$ based on n simulated particles. The true Miles ellipsoid is a prolate ellipsoid with semi-axis lengths $a = 5.866$, $b = c = 4.968$. Estimation is done under the assumption of restricted isotropy minimizing the Frobenius matrix norm.

5 Example

In this example, we illustrate the developed methods, using samples of neurons from layer III of the medial prefrontal cortex (mPFC).

Volume tensor estimation was performed in two mature rats. For each rat, a tissue block containing the mPFC region was embedded in glycol methacrylate (GMA) and cut coronally into parallel 140 μm thick plastic sections. The thick sections were stained with thionin, using the following procedure: first the sections were stained free floating in 10% thionin for 60 min to obtain uniform staining through the whole section, then sections were immersed in distilled water (10 min), thionin (10 min), 96% alcohol (3 min), 99% alcohol (10 min), xylene (15 min) and finally mounted on glass slides and covered with 110 μm thick coverslips.

Two thick sections were selected systematic uniform randomly for further analysis. Each section was analyzed with a systematic set of disectors, resulting in about 100 sampled neurons in each section. The nucleolus of a neuron was used as reference point in the sampling. Figure 7 illustrates the collection of measurements for one sampled neuron. The direction of the vertical axis perpendicular to the surface of the mPFC region is marked as a green line through the nucleolus, see Figure 7a.

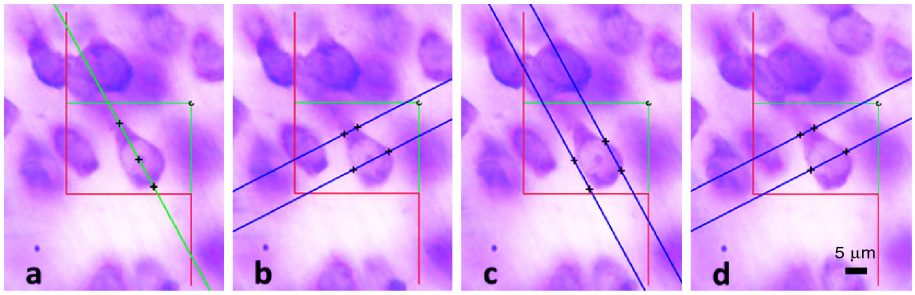

Figure 7: (a) shows the focal plane through the reference point (nucleolus) of a sampled neuron. The reference point is the + in the middle. The green line passing through the reference point is parallel to the vertical axis. The two extreme +'s on this green line indicate the extent of the neuron in this direction. (b)–(d) show the subsampling of the neuron with three systematic planes with distance 1.67 µm between neighbour planes. The distance between pairs of test lines within a plane is 5 µm. The intersection points between the boundary of a neuron and the test lines are indicated by +. The length of the scale bar to the right is 5 µm.

The data have been analyzed under the assumption that the neurons in the mPFC region can be regarded as part of a stationary particle process and the distribution of the neurons is invariant under rotations around an axis perpendicular to the surface of the mPFC region. In Table 3, we show for each rat and section the estimated mean particle volume $\widehat{v}$, the length $\|\widehat{c}\|$ of the estimated displacement vector and the lengths of the semi-axes of the estimated Miles ellipsoid $\widehat{e}$. Recall that, because of the restricted isotropy assumption, $\widehat{e}$ is an ellipsoid of revolution around the vertical axis.

Note that the displacement is rather small compared to the size of the neurons, indicating that the nucleolus of a neuron is centrally positioned within the neuron. Note also that the estimated ellipsoids are elongated in the direction of the vertical axis. As explained in Section 4, the volume of the estimated Miles ellipsoid is equal to the estimated mean particle volume.

The similarity of the estimates obtained on the two sections in a rat gives reason to believe that the assumption of restricted isotropy is reasonable, at least approximately. The hypothesis of isotropy, implying a spherical Miles ellipsoid, was rejected at level 5% by the non-parametric test developed in [12, Section 4.5]

	rat 1		rat 2	
parameter	section 1	section 2	section 1	section 2
volume (µm^3)	473	477	815	710
displacement (µm)	0.19	0.22	0.51	0.22
parallel semi-axis (µm)	5.24	5.17	6.16	5.61
perpendicular semi-axes (µm)	4.64	4.69	5.62	5.50

Table 3: For each rat and section, the table shows the estimated mean particle volume, the length of the estimated displacement vector and the lengths of the semi-axes of the estimated Miles ellipsoid. For more details, see text.

6 Discussion

The developed methods are sensitive to tissue shrinkage. For light microscopy, we usually have four different embedding media: plastic and paraffin to be cut on a microtome, freezing to be cut on a cryostat and agar to be cut on a vibratome. Each of these media have different physical characteristics and will therefore also have different properties with regard to tissue deformation ([5]), which may affect the tensor estimation. Plastic (derivatives of methacrylate) sections, as used in the example in Section 5, are typically subjected to minor tissue deformation in the range of 0–10% shrinkage on a volume basis. This may therefore only have little effect on the tensor estimation, but it is important to keep track of the tissue deformation during infiltration/embedding, cutting and staining. Paraffin sections typically shrink a dramatic 50–60% on a volume basis and to a different degree in the x-, y- and z-axis. It is therefore challenging to try to estimate tensors if such an embedding media is used. Both frozen and vibratome (agar embedding) sections are hardly deformed in the x-

and y-axis but can easily be subjected to 50% shrinkage in the z-axis. If the blocks have been cut on a calibrated cryostat/vibratome and the local section thickness measured, it is possible to correct for the relatively large z-axis tissue shrinkage.

The data for tensor estimation are collected using optical rotators. In contrast to e.g. the spatial rotator design ([7]), this design only uses measurements from the central part of the cells. This is an advantage because in optical microscopy it is often difficult to observe the peripheral parts of the cell due to overprojection effects.

In the application, it was assumed that the distribution of the neurons in the mPFC region is invariant under rotation around an axis perpendicular to the surface of the mPFC region. This assumption made it possible to use the coronal sections in the analysis. However, the data could not give us any information, concerning the orientation of the neurons relative to this axis.

The particle models used in the two simulation studies were qualitatively different with the second model having a similar appearance as the data example considered in Section 5. In the first case, all particles were translates of the same particle. As a consequence, parallel optical rotators through sampled particles contain the same information. Accordingly, it was important to generate a sufficient number of independently rotated vertical slices. Particles generated by the second particle model have a distribution that is invariant under rotation around the vertical axis so here it is not needed to uniformly rotate the optical slices around the vertical axis. A precise estimate of the Miles ellipsoid was obtained based on samples of 100 particles indicating that this number of particles should be sufficient to obtain reliable estimates also in the data example.

Acknowledgements

We are grateful to Kaj Vedel for the skilful technical assistance with the graphical illustrations. We also much appreciate the programming assistance of Sine Flarup Budtz. This work has been supported by Centre for Stochastic Geometry and Advanced Bioimaging, funded by the Villum Foundation.

References

[1] Baddeley, A. and Jensen, E.B.V. (2005): *Stereology for Statisticians.* Chapman & Hall/CRC, Boca Raton.

[2] Beisbart, C., Barbosa, M.S., Wagner, H. and da F. Costa, L. (2006): Extended morphometric analysis of neuronal cells with Minkowski valuations. *Eur. Phys. J. B.* **52**, 531–546.

[3] Beisbart, C., Dahlke, R., Mecke, K.R. and Wagner, H. (2002): Vector- and tensor-valued descriptors for spatial patterns. In *Morphology of Condensed Matter*, Vol. 600 of Lecture Notes in Physics. Springer, Berlin; 249–271.

[4] Denis, E.B., Barat, C., Jeulin, D. and Ducottet, C. (2008): 3D complex shape characterizations by statistical analysis: application to aluminium alloys. *Mater. Charact.* **59**, 338–343.

[5] Dorph-Petersen, K.-A., Nyengaard, J.R. and Gundersen, H.J.G. (2001): Tissue shrinkage and unbiased stereological estimation of particle number and size. *J. Microsc.* **204**, 232–246.

[6] Jensen, E.B.V. (1998): *Local Stereology.* World Scientific, London.

[7] Rasmusson, A., Hahn, U., Larsen, J.O., Gundersen, H.J.G., Jensen, E.B.V. and Nyengaard, J.R. (2013): The spatial rotator. *J. Microsc.* **250**, 88–100.

[8] Schröder-Turk, G.E., Kapfer, S., Breidenbach, B., Beisbart, C. and Mecke, K. (2010): Tensorial Minkowski functionals and anisotropy measures for planar patterns. *J. Microsc.* **238**, 57–74.

[9] Schröder-Turk, G.E., Mickel, W., Kapfer, S.C., Klatt, M.A., Schaller, F.M., Hoffmann, M.J.F., Kleppmann, N., Armstrong, P., Inayat, A., Hug, D., Reichelsdorfer, M., Peukert, W., Schwieger, W. and Mecke, K. (2011): Minkowski tensor shape analysis of cellular, granular and porous structures. *Adv. Mater.* **23**, 2535–2553.

[10] Tandrup, T., Gundersen, H.J.G. and Jensen, E.B.V. (1997): The optical rotator. *J. Microsc.* **186**, 108–120.

[11] Zaidel, D.W., Esiri, M.M. and Harrison, P.J. (1997): Size, shape, and orientation of neurons in the left and right hippocampus: Investigation of normal asymmetries and alterations in schizophrenia. *Am. J. Psychiat.* **154**, 812–818.

[12] Ziegel, J.F., Nyengaard, J.R. and Jensen, E.B.V. (2015): Estimating particle shape and orientation using volume tensors. *Scand. J. Stat.* **42**, 813–831.

Appendix

In this Appendix, we indicate how the g-functions (3.4)-(3.9) can be derived.

In [12], it is shown that a design-unbiased estimator of $T_k(K)$ is

$$\widetilde{T}_k(K) = \frac{1}{k!} \int_{K \cap S_2} x^k F_{1,1}\left(\frac{t^2}{d(x, L_1)^2}\right)^{-1} \mathrm{d}x,$$

$k = 0, 1, 2$, where S_2 is the optical rotator slice, L_1 is the vertical axis, chosen to pass through O, and $d(x, L_1)$ is the distance between x and L_1.

The slice S_2 is now subsampled with a uniformly translated systematic grid of planes, parallel to the central plane L_2 of the slice and with distance Δ_1, say, between neighbour planes. Each such plane is of the form $L_2 + \delta v$, where $\delta \in [-t, t]$ and v is a unit vector perpendicular to L_2. The contribution to $\widetilde{T}_k(K)$ from each such plane is

$$\frac{\Delta_1}{k!} \int_{K \cap (L_2 + \delta v)} x^k F_{1,1}\left(\frac{t^2}{d(x, L_1)^2}\right)^{-1} \mathrm{d}x.$$

These integrals are discretized by a uniformly translated systematic grid of lines in $L_2 + \delta v$ with distance Δ_2, say, between neighbour lines.

Let us first consider the case where the lines are parallel to L_1. Such a line is of the form $L_1 + \delta v + \tau w$ where $w \in L_2$ is a unit vector perpendicular to L_1. The contribution from such a line to $\widetilde{T}_k(K)$ becomes

$$\frac{\Delta_1 \Delta_2}{k!} \int_{K \cap (L_1 + \delta v + \tau w)} x^k F_{1,1} \left(\frac{t^2}{d(x, L_1)^2} \right)^{-1} \mathrm{d}x.$$

In [12], this integral has been determined explicitly for $K \cap (L_1 + \delta v + \tau w)$ an arbitrary line segment $[b_-, b_+]$.

In the other case, the lines in $L_2 + \delta v$ are perpendicular to L_1 and of the form $\mathrm{span}\{w\} + \delta v + \tau u$. The contribution to $\widetilde{T}_k(K)$ from such a line is

$$\frac{\Delta_1 \Delta_2}{k!} \int_{K \cap (\mathrm{span}\{w\} + \delta v + \tau u)} x^k F_{1,1} \left(\frac{t^2}{d(x, L_1)^2} \right)^{-1} \mathrm{d}x.$$

In the case where $K \cap (\mathrm{span}\{w\} + \delta v + \tau u)$ is a line segment, this integral is also simplified in [12].

The g-functions (3.4)-(3.9) can now be derived by using these results for $w = (1, 0, 0)$, $u = (0, 1, 0)$ and $v = (0, 0, 1)$. Note that $a = \Delta_1 \Delta_2$.